Mechanics of Advanced Composite Structures 4 (2017) 47-58

Semnan University

Mechanics of Advanced Composite Structures

journal homepage: http://MACS.journals.semnan.ac.ir


# On the Buckling the Behavior of a Multiphase Smart Plate based on a Higher-order Theory

**S. Razavi**

*Young Researchers and Elite Club, Tabriz Branch, Islamic Azad University, Tabriz, Iran*

**PAPER INFO**

***Paper history:***
Received 2016-09-09
Revised 2016-10-18
Accepted 2016-10-29

***Keywords:***
Analytical solution
Buckling load
Higher-order plate theory
Magneto-electro-elastic coupling
Smart plate

**ABSTRACT**

Magneto-electro-elastic materials are multiphase smart materials that exhibit coupling among electrical, magnetic and mechanical energy fields. Due to this ability, they have been the topic of numerous research in the past decade. In this paper, buckling behavior of a multiphase magneto-electro-elastic rectangular plate with simply supported boundary conditions is investigated, based on Reddy's higher-order shear deformation theory. Gauss's laws for electrostatics and magnetostatics are used to model the electric and magnetic behaviors of the plate. The partial differential equations of motion are reduced to ordinary differential equations by using the Galerkin method. Then, the closed-form expression for the critical buckling load of the plate considered is obtained. Some examples are presented to validate the study and to investigate the effects of some parameters on the critical buckling loads of the multiphase magneto-electro-elastic rectangular plates. It is found that the buckling behavior of the magneto-electro-elastic plate is dominated by the elastic properties of the plate, and magneto-electric coefficients slightly increase the critical buckling load of the plate.

DOI: 10.22075/MACS.2016.485


## 1. Introduction

Magneto-electro-elastic (MEE) materials are a type of smart materials that exhibit coupling among mechanical, electric and magnetic fields, which makes them suitable to be used in sensors and actuators, to control vibrations and to harvest energy, etc.

Various researchers have extensively studied the buckling of isotropic and composite plates. Brunelle [1] studied the buckling of transversely isotropic rectangular plates based on Mindlin's plate theory. Mizusawa [2] and Dawe and Wang [3] used spline strip methods to study the buckling behavior of rectangular plates. Various researchers have used the differential quadrature (DQ) method to investigate the buckling of rectangular plates [4-7]. Wang et al. [8] analyzed the buckling of a thin rectangular plate with nonlinearly distributed loadings along two opposite edges by using the DQ method. Cui et al. [9] investigated the dynamic buckling of imperfect rectangular plates subjected to impact loads. Xiang and Wang [10] determined the exact buckling loads and vibration frequencies of stepped plates by using the classical plate theory (CPT) and the Levy method. Chen and Liew [11] and Wang and Peng [12] used mesh-free approaches to analyze the buckling behavior of functionally graded (FG) and thin isotropic rectangular plates, respectively. Javaheri and Eslami [13] and Matsunaga [14] studied the thermal buckling of FG plates based on the higher-order shear deformation theory (HSDT). Some authors have used finite element models (FEMs) to study the buckling of various plates. Selim and Akbarov [15] studied the buckling instability of a clamped viscoelastic plate by using a three-dimensional (3D) FEM. Ghorbanpour Arani et al. [16] used the FEM and analytical method to analyze the buckling of composite plates reinforced by single-walled carbon nanotubes. Many authors have used analytical methods

* Corresponding author. Tel.: +98-9141051582; Fax: +98-413-4752936

*E-mail address:* soheilrazavi@outlook.com

with different plate theories to investigate the buckling behavior of plates. Mohammadi et al. [17] used CPT and the Levy method to analyze the buckling of FG rectangular plates. Kim et al. [18] and Thai and Kim [19] used a two-variable refined theory with the Navier and Levy methods, respectively, to study the buckling of isotropic and orthotropic plates. Bodaghi and Saidi [20] presented an analytical model for analyzing the buckling of FG rectangular plates based on the HSDT and Levy methods. Sinusoidal [21], inverse trigonometric [22], hyperbolic [23], inverse hyperbolic [24], and exponential [25] shear deformation theories have also been used to model the buckling behavior of composite and FG plates. Fares and Zenkour [26] used various theories to study the buckling and free vibration of laminated rectangular plates. They concluded that the CPT is not suitable even for thin laminates. In addition, they found that the first-order shear deformation theory (FSDT) gives acceptable results for properly chosen shear correction factors. Zenkour [27] investigated the buckling behavior of fiber-reinforced viscoelastic composite plates based on CPT, FSDT, HSDT and the sinusoidal shear deformation theory and then compared the results. He showed that despite the CPT-based results, the results of the FSDT and sinusoidal shear deformation theory agree well with those of the HSDT. Ranjbaran et al. [28] and Cetkovic [29] used layerwise theory to study the buckling of sandwich and laminated plates, respectively. Some authors have also investigated the buckling of piezoelectric structures [30, 31].

Pan [32] studied the static response of the MEE plate for the first time. Since then, many researchers have investigated the static and dynamic responses of these smart structures. Free vibration [33], large deflection [34], nonlinear vibration [35] and vibration control [36] of MEE plates have been studied. Xu et al. [37] studied the surface effects on the bending, buckling and free vibration of MEE beams. Li et al. [38] investigated the buckling and free vibration of the MEE nanobeam, based on the nonlocal theory and the Timoshenko beam theory. Li [39] studied the buckling of the MEE plate resting on a Pasternak foundation by using Mindlin's plate theory. Kumaravel et al. [40] and Lang and Xuewu [41] studied the buckling and free vibration of MEE cylindrical shells. Ansari et al. [42] developed a shear deformable nonlocal model for nonlinear forced vibration analysis of MEE nanobeams. Ebrahimi and Barati [43] presented a size-dependent beam model to study the buckling behavior of curved MEE nanobeams. Jamalpoor et al. [44] investigated the free vibration and buckling of MEE microplates based on modified strain gradient and Kirchhoff plate theories. Farajpour et al. [45] developed a nonlocal model for nonlinear free vibration of MEE nanoplates based on the Kirchhoff plate theory. Xu et al. [46] investigated the bending, buckling and free vibration of MEE beams based on the Euler-Bernoulli beam theory. The FEM [47] and third-order shear deformation theory (TSDT) [48] have also been used to analyze the static and dynamic response of MEE plates. Wenjun et al. [49] introduced a two-dimensional linear theory to analyze the response of MEE plates.

In this paper, the buckling loads of a multiphase MEE rectangular plate with simply supported boundary conditions is investigated based on Reddy's HSDT. Gauss's laws for electrostatics and magnetostatics are used to model the electric and magnetic behaviors of the plate. Then, the closed- form expression for the critical buckling load of the plate considered is obtained. Some examples are presented to study the effects of some parameters on the critical buckling load of these smart plates.

## 2. Problem Modeling

### 2.1. Basic relations

Consider a multiphase MEE plate with the dimensions of $a\times b\times h$ that is subjected to biaxial in-plane loads along its edges, as it is shown in Fig. 1 ($-1\leq\ \zeta\ \leq+1$). The plate is a composite smart plate made of piezoelectric material as the inclusions and magnetostrictive material as the matrix. Based on Reddy's HSDT, the displacement field of this plate is as shown below [50]:

$$u(x,y,z,t)=u_0(x,y,t)+z\,\theta_x(x,y,t)-4z^3\left(\theta_x+w_{0,x}\right)/3h^2 \tag{1}$$

$$v(x,y,z,t)=v_0(x,y,t)+z\,\theta_y(x,y,t)-4z^3\left(\theta_y+w_{0,y}\right)/3h^2 \tag{2}$$

$$w(x,y,z,t)=w_0(x,y,t) \tag{3}$$

where $u_0$, $v_0$ and $w_0$ are the displacements of the midplane along the $x$, $y$ and $z$ directions, respectively, and $\theta_x$ and $\theta_y$ are the rotations of a transverse normal about the $y$ and $x$ directions, respectively.

The constitutive equations of a transversely isotropic MEE plate can be expressed as shown below [32]:

$$\{\sigma\}=[C]\{\varepsilon\}-[e]\{E\}-[q]\{H\} \tag{4}$$

$$\{D\}=[e]^T\{\varepsilon\}+[\eta]\{E\}+[d]\{H\} \tag{5}$$

$$\{B\}=[q]^T\{\varepsilon\}+[d]\{E\}+[\mu]\{H\} \tag{6}$$

where $\{\sigma\}$ is the stress vector, $\{\varepsilon\}$ is the strain vector, $\{D\}$ and $\{B\}$ are the electric displacement and magnetic flux vectors, respectively. $[C]$, $[\eta]$ and $[\mu]$ are the elastic, dielectric and magnetic permeability coefficient matrices, respectively, and $[e]$, $[q]$ and $[d]$ are the piezoelectric, piezomagnetic and magnetoelectric coefficient matrices, respectively.

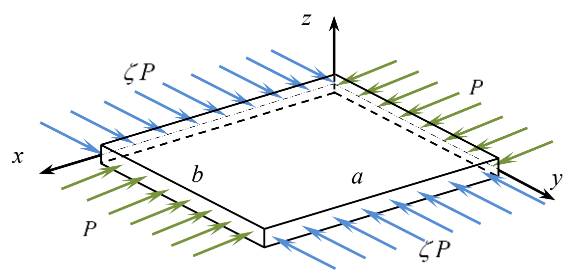


**Figure 1.** Schematic of the MEE plate subjected to in-plane loads.

Based on the HSDT and when transversely isotropic MEE plates with electric and magnetic fields are applied along the $z$-direction, these vectors and matrices are expressed in the following form [32, 50]:

$$[C]=\begin{bmatrix} C_{11} & C_{12} & 0 & 0 & 0 \\ C_{12} & C_{22} & 0 & 0 & 0 \\ 0 & 0 & C_{55} & 0 & 0 \\ 0 & 0 & 0 & C_{44} & 0 \\ 0 & 0 & 0 & 0 & C_{66} \end{bmatrix},$$

$$[e]=\begin{bmatrix} 0 & 0 & e_{31} \\ 0 & 0 & e_{32} \\ 0 & e_{24} & 0 \\ e_{15} & 0 & 0 \\ 0 & 0 & 0 \end{bmatrix}, [\eta]=\begin{bmatrix} \eta_{11} & 0 & 0 \\ 0 & \eta_{22} & 0 \\ 0 & 0 & \eta_{33} \end{bmatrix},$$

$$[q]=\begin{bmatrix} 0 & 0 & q_{31} \\ 0 & 0 & q_{32} \\ 0 & q_{24} & 0 \\ q_{15} & 0 & 0 \\ 0 & 0 & 0 \end{bmatrix}, \ [\mu]=\begin{bmatrix} \mu_{11} & 0 & 0 \\ 0 & \mu_{22} & 0 \\ 0 & 0 & \mu_{33} \end{bmatrix}, \tag{7}$$

$$[d]=\begin{bmatrix} d_{11} & 0 & 0 \\ 0 & d_{22} & 0 \\ 0 & 0 & d_{33} \end{bmatrix},$$

$$\{D\}=\{D_x \quad D_y \quad D_z\}^T, \ \{B\}=\{B_x \quad B_y \quad B_z\}^T$$

$$\{E\}=-\{0 \quad 0 \quad \phi_{,z}\}^T, \quad \{H\}=-\{0 \quad 0 \quad \psi_{,z}\}^T$$

$$\begin{Bmatrix} \varepsilon_x \\ \varepsilon_y \\ \gamma_{xz} \\ \gamma_{yz} \\ \gamma_{xy} \end{Bmatrix}=\begin{Bmatrix} u_{0,x} \\ v_{0,y} \\ \theta_x+w_{0,x} \\ \theta_y+w_{0,y} \\ u_{0,y}+v_{0,x} \end{Bmatrix}+z\begin{Bmatrix} \theta_{x,x} \\ \theta_{y,y} \\ 0 \\ 0 \\ \theta_{x,y}+\theta_{y,x} \end{Bmatrix}- \\ \frac{4}{h^2}z^2\begin{Bmatrix} 0 \\ 0 \\ \theta_x+w_{0,x} \\ \theta_y+w_{0,y} \\ 0 \end{Bmatrix}-\frac{4}{3h^2}z^3\begin{Bmatrix} \theta_{x,x}+w_{0,xx} \\ \theta_{y,y}+w_{0,yy} \\ 0 \\ 0 \\ \theta_{x,y}+\theta_{y,x}+2w_{0,xy} \end{Bmatrix} \tag{8}$$

where $\phi$ and $\psi$ are the electric and magnetic potentials, respectively.

## 2.2. Equations of motion

Based on Reddy's HSDT, the equations of the static motion of the MEE plate are expressed by [50]:

$$N_{x,x}+N_{xy,y}=0 \tag{9}$$

$$N_{xy,x}+N_{y,y}=0 \tag{10}$$

$$\bar{Q}_{x,x}+\bar{Q}_{y,y}+\frac{4}{3h^2}\left(P_{x,xx}+2P_{xy,xy}+P_{y,yy}\right)+ \\ N_x w_{0,xx}+N_y w_{0,yy}=0 \tag{11}$$

$$\bar{M}_{x,x}+\bar{M}_{xy,y}-\bar{Q}_x=0 \tag{12}$$

$$\bar{M}_{xy,x}+\bar{M}_{y,y}-\bar{Q}_y=0, \tag{13}$$

where

$$\bar{M}_x=M_x-\frac{4}{3h^2}P_x, \bar{M}_y=M_y-\frac{4}{3h^2}P_y, \\ \bar{M}_{xy}=M_{xy}-\frac{4}{3h^2}P_{xy}, \\ \bar{Q}_x=Q_x-\frac{4}{h^2}R_x, \quad \bar{Q}_y=Q_y-\frac{4}{h^2}R_y \tag{14}$$

And the resultants are determined by:

$$\{N_{\alpha\beta} \quad M_{\alpha\beta} \quad P_{\alpha\beta}\}=\int_{-h/2}^{h/2}\sigma_{\alpha\beta}\{1 \quad z \quad z^3\}dz, \\ \{Q_\alpha \quad R_\beta\}=\int_{-\frac{h}{2}}^{\frac{h}{2}}\sigma_{\alpha z}\{1 \quad z^2\}dz, \quad (\alpha,\beta=x,y) \tag{15}$$

To obtain the resultants of Eq. (15) and then the parameters of Eq. (14), $\phi_{,z}$ and $\psi_{,z}$, which are introduced in Eq. (7), must be determined first. To do this, Gauss's laws for electrostatics and magnetostatics, with the magneto-electric (ME) boundary condition on bottom and upper surfaces of the MEE plate, are used here. Thus, using

$$D_{x,x}+D_{y,y}+D_{z,z}=0 \\ B_{x,x}+B_{y,y}+B_{z,z}=0 \tag{16}$$

one obtains the following expressions for $\phi_{,z}$ and $\psi_{,z}$:

$$\phi_{,z}=\frac{1}{3}(\lambda_1A_3+\lambda_2A_1)z^3+(\lambda_1A_4+\lambda_2A_2)z+\phi_0 \\ \psi_{,z}=\frac{1}{3}(\lambda_1A_1+\lambda_3A_3)z^3+(\lambda_1A_2+\lambda_3A_4)z+\psi_0 \tag{17}$$

where

$$\lambda_1=d_{33}/\left(d_{33}^2-\eta_{33}\mu_{33}\right), \lambda_2=-\mu_{33}/\left(d_{33}^2-\eta_{33}\mu_{33}\right), \\ \lambda_3=-\eta_{33}/\left(d_{33}^2-\eta_{33}\mu_{33}\right) \tag{18}$$

$$A_1=\frac{-4}{h^2}\left[e_{24}\left(\theta_{x,y}+w_{0,xy}\right)+e_{31}\left(\theta_{x,x}+w_{0,xx}\right)+ \right. \\ \left. e_{15}\left(\theta_{y,x}+w_{0,xy}\right)+e_{32}\left(\theta_{y,y}+w_{0,yy}\right)\right] \\ A_2=e_{24}\left(\theta_{x,y}+w_{0,xy}\right)+e_{15}\left(\theta_{y,x}+w_{0,xy}\right)+ \\ e_{31}\theta_{x,x}+e_{32}\theta_{y,y} \\ A_3=\frac{-4}{h^2}\left[q_{24}\left(\theta_{x,y}+w_{0,xy}\right)+q_{31}\left(\theta_{x,x}+w_{0,xx}\right)+ \right. \\ \left. q_{15}\left(\theta_{y,x}+w_{0,xy}\right)+q_{32}\left(\theta_{y,y}+w_{0,yy}\right)\right] \\ A_4=q_{24}\left(\theta_{x,y}+w_{0,xy}\right)+q_{15}\left(\theta_{y,x}+w_{0,xy}\right)+ \\ q_{31}\theta_{x,x}+q_{32}\theta_{y,y} \tag{19}$$

In Eq. (17), $\phi_0$ and $\psi_0$ are the constants of integration and are obtained by using ME boundary condition, which is assumed as below:

$$\begin{aligned} &\phi=0, \quad \psi=0 \quad (z=-h/2) \\ &\phi=V_0, \quad \psi=\Omega_0 \quad (z=h/2) \end{aligned} \tag{20}$$

where $V_0$ is the electric potential and $\Omega_0$ is the magnetic potential that are applied to the upper surface of the MEE plate. Eqs. (17) and (20) give $\phi_0 = V_0/h$ and $\psi_0 = \Omega_0/h$.

Thus, Eqs. (4), (7), (8), (15) and (17) give the resultants:

$$\begin{aligned} N_x &= h\left(C_{11}u_{0,x}+C_{12}v_{0,y}\right)+e_{31}V_0+q_{31}\Omega_0-P \\ N_y &= h\left(C_{12}u_{0,x}+C_{22}v_{0,y}\right)+e_{32}V_0+q_{32}\Omega_0-\zeta P \\ N_{xy} &= hC_{66}\left(u_{0,y}+v_{0,x}\right) \end{aligned} \tag{21}$$

$$\begin{aligned} Q_x &= \frac{2h}{3}C_{55}\left(w_{0,x}+\theta_x\right),\ R_x=\frac{h^2}{20}Q_x, \\ Q_y &= \frac{2h}{3}C_{44}\left(w_{0,y}+\theta_y\right),\ R_y=\frac{h^2}{20}Q_y \end{aligned} \tag{22}$$

$$\begin{aligned} M_x = \frac{h^3}{12}&\Big[C_{11}\theta_{x,x}+C_{12}\theta_{y,y}+e_{31}\left(\lambda_1A_4+\lambda_2A_2\right)+ \\ &q_{31}\left(\lambda_1A_2+\lambda_3A_4\right)\Big]+ \\ &\frac{h^5}{80}\Big[-\frac{4}{3h^2}C_{11}\left(\theta_{x,x}+w_{0,xx}\right)- \\ &\frac{4}{3h^2}C_{12}\left(\theta_{y,y}+w_{0,yy}\right)+ \\ &\frac{1}{3}e_{31}\left(\lambda_1A_3+\lambda_2A_1\right)+\frac{1}{3}q_{31}\left(\lambda_1A_1+\lambda_3A_3\right)\Big] \end{aligned} \tag{23}$$

$$\begin{aligned} M_y = \frac{h^3}{12}&\Big[C_{12}\theta_{x,x}+C_{22}\theta_{y,y}+e_{32}\left(\lambda_1A_4+\lambda_2A_2\right)+ \\ &q_{32}\left(\lambda_1A_2+\lambda_3A_4\right)+ \\ &\frac{h^5}{80}\Big[-\frac{4}{3h^2}C_{12}\left(\theta_{x,x}+w_{0,xx}\right)- \\ &\frac{4}{3h^2}C_{22}\left(\theta_{y,y}+w_{0,yy}\right)+ \\ &\frac{1}{3}e_{32}\left(\lambda_1A_3+\lambda_2A_1\right)+\frac{1}{3}q_{32}\left(\lambda_1A_1+\lambda_3A_3\right)\Big] \end{aligned} \tag{24}$$

$$M_{xy}=\frac{h^3}{15}C_{66}\left(\theta_{x,y}+\theta_{y,x}\right)-\frac{h^3}{30}C_{66}w_{0,xy} \tag{25}$$

$$\begin{aligned} P_x = \frac{h^5}{80}&\Big[C_{11}\theta_{x,x}+C_{12}\theta_{y,y}+e_{31}\left(\lambda_1A_4+\lambda_2A_2\right)+ \\ &q_{31}\left(\lambda_1A_2+\lambda_3A_4\right)\Big]+ \\ &\frac{h^7}{448}\Big[-\frac{4}{3h^2}C_{11}\left(\theta_{x,x}+w_{0,xx}\right)- \\ &\frac{4}{3h^2}C_{12}\left(\theta_{y,y}+w_{0,yy}\right)+ \\ &\frac{1}{3}e_{31}\left(\lambda_1A_3+\lambda_2A_1\right)+\frac{1}{3}q_{31}\left(\lambda_1A_1+\lambda_3A_3\right)\Big] \end{aligned} \tag{26}$$

$$\begin{aligned} P_y = \frac{h^5}{80}&\Big[C_{12}\theta_{x,x}+C_{22}\theta_{y,y}+e_{32}\left(\lambda_1A_4+\lambda_2A_2\right)+ \\ &q_{32}\left(\lambda_1A_2+\lambda_3A_4\right)\Big]+ \\ &\frac{h^7}{448}\Big[-\frac{4}{3h^2}C_{12}\left(\theta_{x,x}+w_{0,xx}\right)- \\ &\frac{4}{3h^2}C_{22}\left(\theta_{y,y}+w_{0,yy}\right)+ \\ &\frac{1}{3}e_{32}\left(\lambda_1A_3+\lambda_2A_1\right)+\frac{1}{3}q_{32}\left(\lambda_1A_1+\lambda_3A_3\right)\Big] \end{aligned} \tag{27}$$

$$P_{xy}=\frac{h^5}{105}C_{66}\left(\theta_{x,y}+\theta_{y,x}\right)-\frac{h^5}{168}C_{66}w_{0,xy} \tag{28}$$

where the in-plane boundary loads have been included in the in-plane force resultants of Eq. (21).

Substituting Eqs. (14) and (21) – (28) into Eqs. (9) – (13) gives the equations of motion in terms of the displacements and rotations of the midplane of the plate:

$$C_{11}u_{0,xx}+C_{66}u_{0,yy}+\left(C_{12}+C_{66}\right)v_{0,xy}=0 \tag{29}$$

$$C_{66}v_{0,xx}+C_{22}v_{0,yy}+\left(C_{12}+C_{66}\right)u_{0,xy}=0 \tag{30}$$

$$\begin{aligned} &L_1w_{0,xx}+L_2w_{0,yy}+L_4\theta_{x,x}+L_5\theta_{y,y}+L_6\theta_{x,xxx}+ \\ &L_7\theta_{y,xxy}+L_8w_{0,xxxx}+L_9\left(\theta_{x,xxy}+w_{0,xxxy}\right)+L_{10}w_{0,xxyy} \\ &+L_{11}\left(\theta_{y,xxx}+w_{0,xxxy}\right)+L_{12}\theta_{x,xyy}+L_{13}\theta_{y,yyy}+ \\ &L_{14}w_{0,yyyy}+L_{15}w_{0,xyyy}+L_{16}\theta_{x,yyy}+L_{17}\theta_{y,xyy}=0 \end{aligned} \tag{31}$$

$$\begin{aligned} &L_{18}w_{0,xxx}+L_{19}w_{0,xyy}+L_{20}w_{0,xxy}+ \\ &\quad L_{21}\left(w_{0,x}+\theta_x\right)+L_{22}\theta_{x,xy}+L_{23}\theta_{y,xx}+ \\ &\quad\quad L_{24}\theta_{x,yy}+L_{25}\theta_{x,xx}+L_{26}\theta_{y,xy}=0 \end{aligned} \tag{32}$$

$$\begin{aligned} &L_{27}w_{0,xxy}+L_{28}w_{0,yyy}+L_{29}w_{0,xyy}+ \\ &\quad L_{30}\left(w_{0,y}+\theta_y\right)+L_{31}\theta_{x,xy}+L_{32}\theta_{y,yy}+ \\ &\quad\quad L_{33}\theta_{x,yy}+L_{34}\theta_{y,xy}+L_{24}\theta_{y,xx}=0 \end{aligned} \tag{33}$$

where $L_i$ ($i$=1,2,…,34) are the constant coefficients and are given in Appendix A.

### 2.3. Determining the critical buckling load

It can be seen that Eqs. (29) and (30) are decoupled from Eqs. (31) – (33). Therefore, to study the buckling behavior of the plate, it is sufficient to consider only Eqs. (31) – (33). For the simply supported boundary condition, the following relations hold:

$$\begin{aligned} &w_0=w_{0,xx}=\theta_y=0 \quad \text{at} \quad (x=0,a) \\ &w_0=w_{0,yy}=\theta_x=0 \quad \text{at} \quad (y=0,b) \end{aligned} \tag{34}$$

Therefore, the transverse displacement and the rotations can be determined by:

$$\begin{aligned} w_0 &= hW\ \sin\left(m\pi x/a\right)\sin\left(n\pi y/b\right) \\ \theta_x &= X\ \cos\left(m\pi x/a\right)\sin\left(n\pi y/b\right) \\ \theta_y &= Y\ \sin\left(m\pi x/a\right)\cos\left(n\pi y/b\right) \end{aligned} \tag{35}$$

where $W$, $X$, and $Y$ are the amplitudes of the transverse displacement and rotations, and ($m$,$n$) denotes the mode of the plate.

Substituting Eq. (35) into Eqs. (31) to (33) and then using the orthogonality of the trigonometric functions, one obtains the following set of ordinary differential equations:

$$\begin{bmatrix} \gamma_1 & \gamma_2 & \gamma_3 \\ \gamma_4 & \gamma_5 & \gamma_6 \\ \gamma_7 & \gamma_8 & \gamma_9 \end{bmatrix} \begin{Bmatrix} W \\ X \\ Y \end{Bmatrix} = \begin{Bmatrix} 0 \\ 0 \\ 0 \end{Bmatrix} \tag{36}$$

where the components of the coefficient matrix are given in Appendix B. To have a nontrivial solution for Eq. (36), the determinant of the coefficient matrix must equal zero. That is,

$$\begin{vmatrix} \gamma_1 & \gamma_2 & \gamma_3 \\ \gamma_4 & \gamma_5 & \gamma_6 \\ \gamma_7 & \gamma_8 & \gamma_9 \end{vmatrix} = 0 \tag{37}$$

Solving Eq. (37) gives the critical buckling load of the multiphase MEE plate.

## 3. Examples and Discussion

In this section, numerical examples are presented to validate the proposed model and to investigate the effects of some parameters on the critical buckling load of the multiphase MEE plate. As the first comparison, an isotropic square plate is considered and its dimensionless critical buckling loads are determined for different length-to-thickness ($a/h$) ratios in the uniaxial ($\zeta$ = 0) and biaxial ($\zeta$ = +1) compressions. The results are shown in Table 1, with the results based on various plate theories, where RPT denotes the refined plate theory. The dimensionless critical buckling loads of orthotropic plates with different $a/h$ and $b/a$ ratios and different degrees of orthotropy ($E_1/E_2$) are also determined, and the results are shown in Tables 2 and 3. The results are compared with those based on the FSDT, HSDT and exponential shear deformation theory (ESDT), where the error is obtained by using, $error\ (\%) = (Present - HSDT) \times 100/HSDT$.

The dimensionless critical buckling loads in Tables 1 to 3 are determined by using $P^* = P_{cr}a^2/E_2h^3$. The material properties of the orthotropic plate are: $E_1/E_2$ = open, $G_{12} = G_{13} = 0.5, E_2$, $G_{23} = 0.2\ E_2$ and $\nu_{12}$ = 0.25. It is seen that the present model accurately predicts the critical buckling loads of isotropic and orthotropic plates. As the last comparison, the dimensionless critical buckling loads of a square MEE plate are determined and compared with those by Li [39], which are based on Mindlin's plate theory.

The material properties of the multiphase MEE plate are [39, 51]: $C_{11}$ = 226 GPa, $C_{12}$ = 124 GPa, $C_{22}$ = 216 GPa, $C_{44} = C_{55}$ = 44 GPa, $C_{66}$ = 51 GPa, $e_{31} = e_{32}$ = −2.2 C/m$^2$, $e_{15} = e_{24}$ = 0, $q_{31} = q_{32}$ = 290.2 N/Am, $q_{15} = q_{24}$ = 0, $d_{33}$ = 2737.5×10$^{-12}$ Ns/VC, $\eta_{33}$ = 6.35×10$^{-9}$ C$^2$/Nm$^2$ and $\mu_{33}$ = 83.5×10$^{-6}$ Ns$^2$/C$^2$. The critical buckling loads of the MEE plate are normalized by using $P^* = P_{cr}a^2/h^3C_{11}$ and are shown in Table 4. The discrepancy between the results of the present approach and Li's [39] results are computed by, $discrepancy\ (\%) = (Present - Li\ [39]) \times 100/Li\ [39]$.

**Table 1.** Comparison of the dimensionless critical buckling load of a square isotropic plate ($\nu$ = 0.3).

| $\zeta$ | Method | $a/h$ | | | |
|---|---|---|---|---|---|
| | | 5 | 10 | 50 | 100 |
| 0 | RPT [18] | 2.9512 | 3.4224 | 3.6071 | 3.6132 |
| | FSDT* | 2.9498 | 3.4222 | 3.6071 | 3.6132 |
| | CPT* | - | - | - | 3.6152 |
| | Present | 2.9512 | 3.4224 | 3.6071 | 3.6132 |
| +1 | RPT [18] | 1.4756 | 1.7112 | 1.8036 | 1.8066 |
| | FSDT* | 1.4749 | 1.7111 | 1.8036 | 1.8066 |
| | CPT* | - | - | - | 1.8076 |
| | Present | 1.4756 | 1.7112 | 1.8036 | 1.8066 |

* reported by Kim et al. [18]

**Table 2.** Comparison of the dimensionless critical buckling load of square orthotropic plates ($\zeta$ = 0).

| $a/h$ | Method | $E_1/E_2$ | | | |
|---|---|---|---|---|---|
| | | 3 | 10 | 20 | 30 |
| 5 | FSDT* | 3.9386 | 6.1804 | 7.7450 | 8.5848 |
| | HSDT* | 3.9434 | 6.2072 | 7.8292 | 8.7422 |
| | ESDT [25] | 3.9650 | 6.3014 | 8.0946 | 9.2166 |
| | Present | 3.9435 | 6.2071 | 7.8293 | 8.7422 |
| | Error (%) | +0.003 | −0.002 | +0.001 | 0.000 |
| 20 | FSDT* | 5.2994 | 10.620 | 17.662 | 24.102 |
| | HSDT* | 5.2994 | 10.621 | 17.664 | 24.108 |
| | ESDT [25] | 5.3004 | 10.625 | 17.681 | 24.146 |
| | Present | 5.2995 | 10.620 | 17.664 | 24.108 |
| | Error (%) | +0.002 | −0.009 | 0.000 | 0.000 |
| 100 | FSDT* | 5.4206 | 11.142 | 19.309 | 27.448 |
| | HSDT* | 5.4192 | 11.139 | 19.307 | 27.446 |
| | ESDT [25] | 5.4196 | 11.400 | 19.308 | 27.447 |
| | Present | 5.4197 | 11.140 | 19.308 | 27.446 |
| | Error (%) | +0.009 | +0.009 | +0.005 | 0.000 |

* reported by Sayyad and Ghugal [25]

**Table 3.** Comparison of the dimensionless critical buckling load of rectangular orthotropic plates ($\zeta$ = 0, $E_1/E_2$ = 40, $a/h$ = 5).

| Method | $b/a$ | | | | |
|---|---|---|---|---|---|
| | 1.0 | 1.5 | 2.0 | 3.0 | 4.0 |
| FSDT* | 9.1084 | 8.3237 | 8.1178 | 7.9958 | 7.9585 |
| HSDT* | 9.3472 | 8.5541 | 8.3455 | 8.2217 | 8.1837 |
| Present | 9.3472 | 8.5541 | 8.3455 | 8.2217 | 8.1837 |

* reported by Sayyad and Ghugal [25]

**Table 4.** Comparison of the dimensionless critical buckling load of a square MEE plate.

| $\zeta$ | Method | $a/h$ | | | |
|---|---|---|---|---|---|
| | | 5 | 10 | 20 | 1000 |
| 0 | Li [39] | 2.3264 | 2.9747 | 3.1975 | 3.2794 |
| | Present | 2.3384 | 2.9786 | 3.1985 | 3.2793 |
| | Discrepancy(%) | +0.516 | +0.131 | +0.031 | −0.003 |
| +0.5 | Li [39] | 1.5509 | 1.9831 | 2.1317 | 2.1862 |
| | Present | 1.5590 | 1.9858 | 2.1324 | 2.1862 |
| | Discrepancy(%) | +0.522 | +0.136 | +0.033 | 0.000 |
| −0.5 | Li [39] | 4.6527 | 5.9494 | 6.3950 | 6.5587 |
| | Present | 4.6769 | 5.9573 | 6.3971 | 6.5586 |
| | Discrepancy(%) | +0.520 | +0.133 | +0.033 | −0.002 |

It is seen in Tables 1 to 3 that the FSDT cannot accurately predict the critical buckling loads for thick plates ($a/h$ = 5) compared with the present HSDT-based formulation. Moreover, to obtain accurate results from the FSDT, a proper shear correction factor must be chosen [26], which is still an unresolved issue for composite structures [50].

In Table 5, the dimensionless critical buckling loads of rectangular MEE plates are presented for uniaxial and biaxial compression cases. Table 5 shows that for higher aspect ratios, the dimensionless critical buckling load increases. Moreover, in biaxial compression, the dimensionless critical buckling load is smaller.

Fig. 2 shows the dimensionless critical buckling curves for piezoelectric $BaTiO_3$ (barium titanate), magnetostrictive $CoFe_2O_4$ (cobalt ferrite) and MEE square plates. The material properties of $BaTiO_3$ are [52]: $C_{11}$ = 166 GPa, $C_{12}$ = 77 GPa, $C_{22}$ = 166 GPa, $C_{44}$ = $C_{55}$ = 43 GPa, $C_{66}$ = 44.5 GPa, $e_{31}$ = $e_{32}$ = −4.4 C/m$^2$, $e_{15}$ = $e_{24}$ = 11.6 C/m$^2$, $\eta_{33}$ = 12.6×10$^{-9}$ C$^2$/Nm$^2$ and $\mu_{33}$ = 10×10$^{-6}$ Ns$^2$/C$^2$; and for $CoFe_2O_4$, the material properties are: $C_{11}$ = 286 GPa, $C_{12}$ = 173 GPa, $C_{22}$ = 286 GPa, $C_{44}$ = $C_{55}$ = 45.3 GPa, $C_{66}$ = 56.5 GPa, $q_{31}$ = $q_{32}$ = 580.3 N/Am, $q_{15}$ = $q_{24}$ = 550 N/Am, $\eta_{33}$ = 0.093×10$^{-9}$ C$^2$/Nm$^2$ and $\mu_{33}$ = 157×10$^{-6}$ Ns$^2$/C$^2$. It is seen that $BaTiO_3$ has the smallest stiffness coefficient among these smart plates, which is why its dimensionless critical buckling load is smaller for a fixed value of $a/h$ ratio. The dimensionless critical buckling curves of the MEE plate and its equivalent non-magneto-electric (non-MEE) plate are shown in Fig 3. In this figure, non-MEE denotes the MEE plate with $e_{31}$ = $e_{32}$ = $q_{31}$ = $q_{32}$ = $d_{33}$ = $\eta_{33}$ = $\mu_{33}$ = 0. It is seen that the ME coefficients slightly increase the dimensionless critical buckling load. In addition, the buckling behavior of the MEE plate is dominated by the elastic properties of the plate. Figs 4 and 5 show the effects of the electric and magnetic potentials on the dimensionless critical buckling loads of MEE plates. It is seen that using negative electric potentials or positive magnetic potentials leads to higher dimensionless critical buckling loads for MEE rectangular plates.

**Table 5.** The dimensionless critical buckling load of a rectangular MEE plate ($a/h$ = 5).

| $\zeta$ | $a/b$ | | | |
|---|---|---|---|---|
| | 0.5 | 1.0 | 1.5 | 2.0 |
| 0 | 1.0308 | 2.3384 | 5.2095 | 10.164 |
| +1 | 0.8247 | 1.1692 | 1.6029 | 2.0327 |

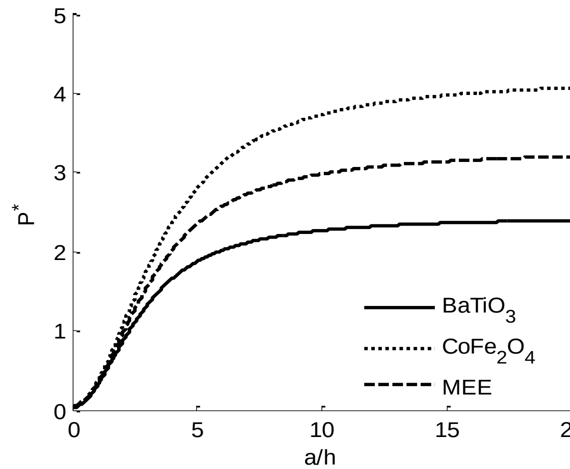


**Figure 2.** The dimensionless critical buckling load curves for different smart square plates ($\zeta$ = 0).

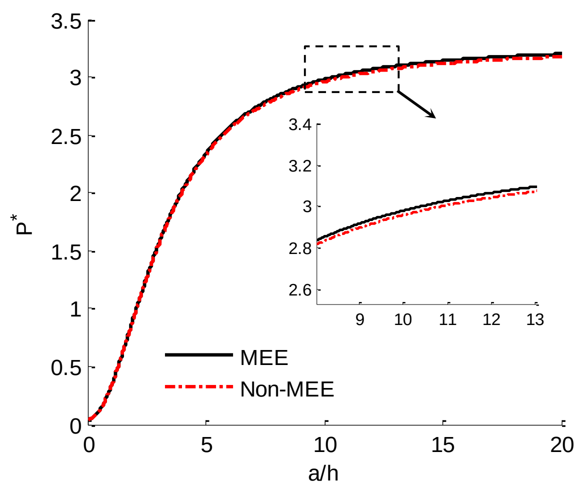


**Figure 3.** The dimensionless critical buckling load curves of an MEE and its equivalent non-ME square plates ($\zeta$ = 0).

In the last example, an MEE square plate with a fixed $a/h$ ratio is considered with a nonzero magneto-electric boundary condition.

Fig 6 shows the result and shows that for MEE plates with smaller thicknesses, the electric and magnetic potentials have considerable effect on the dimensionless critical buckling load. However, as the plate becomes thicker, the effect of the potentials on dimensionless critical buckling decreases dramatically.

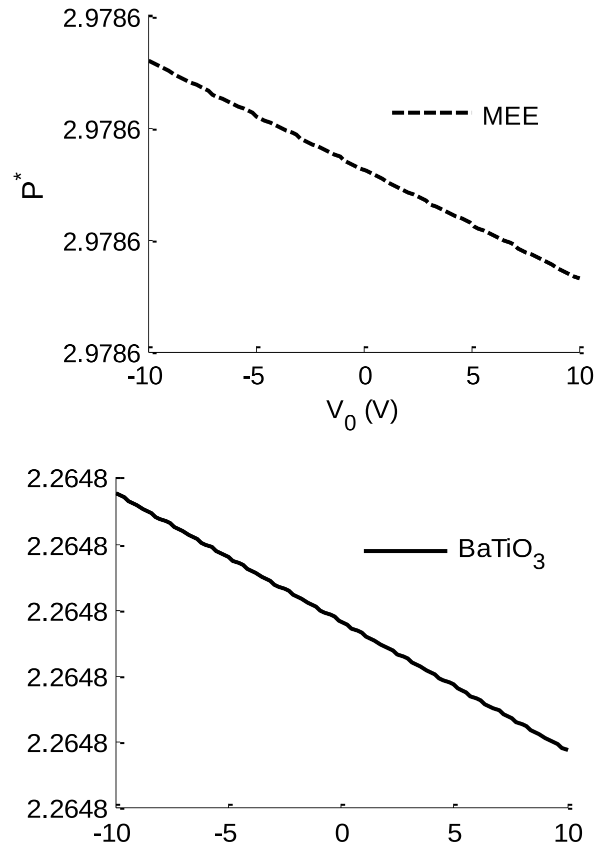


**Figure 4.** The effect of electric potential on the dimensionless critical buckling load of MEE and $BaTiO_3$ square plates ($a/h$ = 10, $\zeta$ = 0).

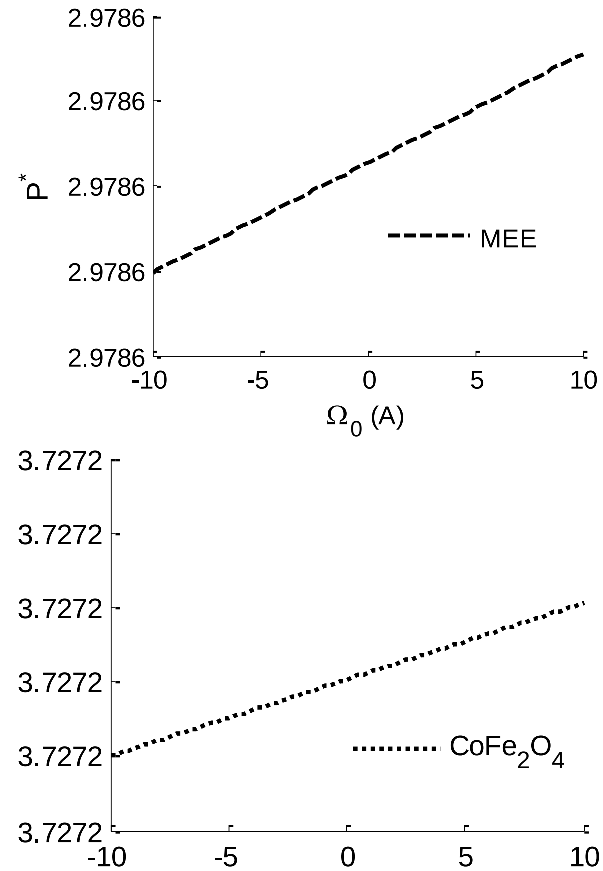


**Figure 5.** The effect of the magnetic potential on the dimensionless critical buckling load of MEE and $CoFe_2O_4$ square plates ($a/h$ = 10, $\zeta$ = 0).

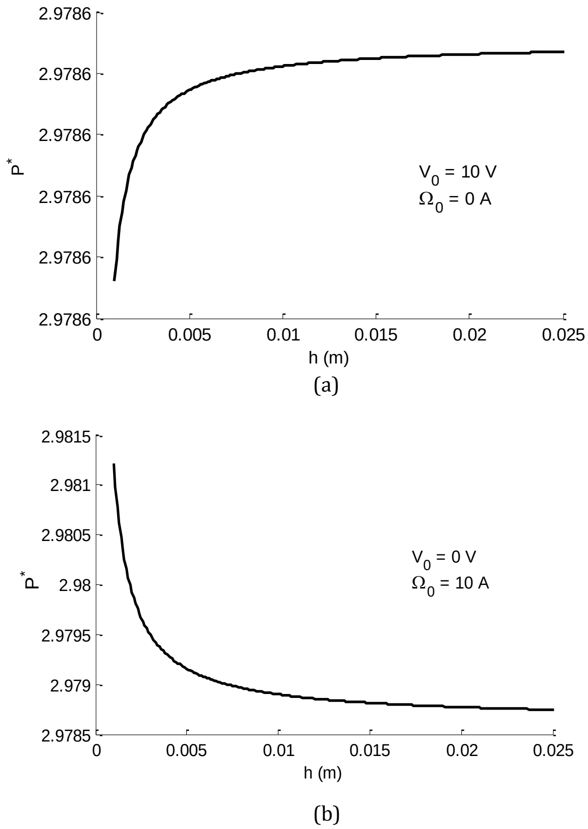


**Figure 6.** The effect of the thickness value on the dimensionless critical buckling load of an MEE square plate when: (a) an electric potential and (b) a magnetic potential are applied to the top surface of the plate ($a/h$ = 10, $\zeta$ = 0).

## 3. Conclusions

The buckling behavior of a multiphase MEE rectangular plate with simply supported boundary conditions was investigated analytically, based on Reddy's higher-order shear deformation theory, Gauss's laws for electrostatics and magnetostatics, and the Galerkin method. Numerical examples were presented and it was found that: (a) in biaxial compression, the dimensionless critical buckling load of the MEE plate was smaller, (b) for a fixed value of the $a/h$ ratio, the piezoelectric $BaTiO_3$ had a smaller dimensionless critical buckling load compared with that of an MEE plate due to its smaller stiffness coefficients, (c) the ME properties of the MEE plate increased the dimensionless critical buckling load of the plate, because the ME effects increased the effective stiffnesses of the MEE plate, and (d) for a fixed value of the $a/h$ ratio, the dimensionless critical buckling loads of MEE plates with smaller thickness values changed considerably with the change in electric or magnetic potentials.

## Nomenclature

| | |
|---|---|
| $a, b, h$ | Length, width and thickness of the plate |
| $C, \eta, \mu$ | Elastic, dielectric and magnetic permeability coefficient matrices |
| **D**, **B** | Electric displacement and magnetic flux vectors |
| **E**, **H** | Electric field and magnetic field vectors |
| $e, q, d$ | Piezoelectric, piezomagnetic and magnetoelectric coefficient matrices |
| **M**, **P** | Moment resultants vectors |
| **N** | In-plane force resultants vector |
| $P$ | In-plane load applied to edge of plate |
| $P_{cr}$ | Critical buckling load |
| $P^*$ | Dimensionless critical buckling load |
| **Q**, **R** | Transverse force resultants vectors |
| $u_0, v_0, w_0$ | Displacements of the midplane along $x$, $y$ and $z$ directions |
| $V_0, \Omega_0$ | Electric and magnetic potentials |
| $W, X, Y$ | Amplitudes of transverse displacement and rotations |
| $\theta_x, \theta_y$ | Rotations of a transverse normal about the $y$ and $x$ directions |
| **σ**, **ε** | Stress and strain vectors |
| $\phi, \psi$ | Electric and magnetic potentials |

## Appendix A

$$L_1 = \frac{8h}{15} C_{55} + e_{31} V_0 + q_{31} \Omega_0 - P$$
$$L_2 = \frac{8h}{15} C_{44} + e_{32} V_0 + q_{32} \Omega_0 - \zeta P \tag{A.1}$$

$$L_4 = \frac{8h}{15} C_{55}, \qquad L_5 = \frac{8h}{15} C_{44}$$

$$L_6 = \frac{4h^3}{315} \left[ C_{11} + e_{31} \left( e_{31} \lambda_2 + q_{31} \lambda_1 \right) + q_{31} \left( e_{31} \lambda_1 + q_{31} \lambda_3 \right) \right] \tag{A.2}$$

$$L_7 = \frac{4h^3}{315} \left[ C_{12} + 2C_{66} + e_{32} \left( e_{31} \lambda_2 + q_{31} \lambda_1 \right) + q_{32} \left( e_{31} \lambda_1 + q_{31} \lambda_3 \right) \right] \tag{A.3}$$

$$L_8 = -\frac{h^3}{252} \left[ C_{11} + e_{31} \left( e_{31} \lambda_2 + q_{31} \lambda_1 \right) + q_{31} \left( e_{31} \lambda_1 + q_{31} \lambda_3 \right) \right] \tag{A.4}$$

$$L_9 = \frac{4h^3}{315} \left[ e_{24} \left( e_{31} \lambda_2 + q_{31} \lambda_1 \right) + q_{24} \left( e_{31} \lambda_1 + q_{31} \lambda_3 \right) \right] \tag{A.5}$$

$$L_{10} = -\frac{h^3}{252} \left[ 2C_{12} + 4C_{66} + e_{32} \left( e_{31} \lambda_2 + q_{31} \lambda_1 \right) + q_{32} \left( e_{31} \lambda_1 + q_{31} \lambda_3 \right) + e_{31} \left( e_{32} \lambda_2 + q_{32} \lambda_1 \right) + q_{31} \left( e_{32} \lambda_1 + q_{32} \lambda_3 \right) \right] \tag{A.6}$$

$$L_{11}=\frac{4h^3}{315}\left[e_{15}\left(e_{31}\lambda_2+q_{31}\lambda_1\right)+q_{15}\left(e_{31}\lambda_1+q_{31}\lambda_3\right)\right] \quad (A.7)$$

$$L_{12}=\frac{4h^3}{315}\left[C_{12}+2C_{66}+e_{31}\left(e_{32}\lambda_2+q_{32}\lambda_1\right)+q_{31}\left(e_{32}\lambda_1+q_{32}\lambda_3\right)\right] \quad (A.8)$$

$$L_{13}=\frac{4h^3}{315}\left[C_{22}+e_{32}\left(e_{32}\lambda_2+q_{32}\lambda_1\right)+q_{32}\left(e_{32}\lambda_1+q_{32}\lambda_3\right)\right] \quad (A.9)$$

$$L_{14}=-\frac{h^3}{252}\left[C_{22}+e_{32}\left(e_{32}\lambda_2+q_{32}\lambda_1\right)+q_{32}\left(e_{32}\lambda_1+q_{32}\lambda_3\right)\right] \quad (A.10)$$

$$L_{15}=\frac{4h^3}{315}\left[e_{24}\left(e_{32}\lambda_2+q_{32}\lambda_1\right)+e_{15}\left(e_{32}\lambda_2+q_{32}\lambda_1\right)+q_{24}\left(e_{32}\lambda_1+q_{32}\lambda_3\right)+q_{15}\left(e_{32}\lambda_1+q_{32}\lambda_3\right)\right] \quad (A.11)$$

$$L_{16}=\frac{4h^3}{315}\left[e_{24}\left(e_{32}\lambda_2+q_{32}\lambda_1\right)+q_{24}\left(e_{32}\lambda_1+q_{32}\lambda_3\right)\right] \quad (A.12)$$

$$L_{17}=\frac{h^3}{315}\left[e_{15}\left(e_{32}\lambda_2+q_{32}\lambda_1\right)+q_{15}\left(e_{32}\lambda_1+q_{32}\lambda_3\right)\right] \quad (A.13)$$

$$L_{18}=-\frac{4h^3}{315}\left[C_{11}+e_{31}\left(e_{31}\lambda_2+q_{31}\lambda_1\right)+q_{31}\left(e_{31}\lambda_1+q_{31}\lambda_3\right)\right] \quad (A.14)$$

$$L_{19}=-\frac{4h^3}{315}\left[C_{12}+2C_{66}+e_{32}\left(e_{31}\lambda_2+q_{31}\lambda_1\right)+q_{32}\left(e_{31}\lambda_1+q_{31}\lambda_3\right)\right] \quad (A.15)$$

$$L_{20}=\frac{17h^3}{315}\left[e_{24}\left(e_{31}\lambda_2+q_{31}\lambda_1\right)+e_{15}\left(e_{31}\lambda_2+q_{31}\lambda_1\right)+q_{24}\left(e_{31}\lambda_1+q_{31}\lambda_3\right)+q_{15}\left(e_{31}\lambda_1+q_{31}\lambda_3\right)\right] \quad (A.16)$$

$$L_{21}=-\frac{8h}{15}C_{55}$$
$$L_{22}=\frac{17h^3}{315}\left[e_{24}\left(e_{31}\lambda_2+q_{31}\lambda_1\right)+q_{24}\left(e_{31}\lambda_1+q_{31}\lambda_3\right)\right] \quad (A.17)$$

$$L_{23}=\frac{17h^3}{315}\left[e_{15}\left(e_{31}\lambda_2+q_{31}\lambda_1\right)+q_{15}\left(e_{31}\lambda_1+q_{31}\lambda_3\right)\right]$$
$$L_{24}=\frac{17h^3}{315}C_{66} \quad (A.18)$$

$$L_{25}=\frac{17h^3}{315}\left[C_{11}+e_{31}\left(e_{31}\lambda_2+q_{31}\lambda_1\right)+q_{31}\left(e_{31}\lambda_1+q_{31}\lambda_3\right)\right] \quad (A.19)$$

$$L_{26}=\frac{17h^3}{315}\left[C_{12}+C_{66}+e_{32}\left(e_{31}\lambda_2+q_{31}\lambda_1\right)+q_{32}\left(e_{31}\lambda_1+q_{31}\lambda_3\right)\right] \quad (A.20)$$

$$L_{27}=-\frac{4h^3}{315}\left[C_{12}+2C_{66}+e_{31}\left(e_{32}\lambda_2+q_{32}\lambda_1\right)+q_{31}\left(e_{32}\lambda_1+q_{32}\lambda_3\right)\right] \quad (A.21)$$

$$L_{28}=-\frac{4h^3}{315}\left[C_{22}+e_{32}\left(e_{32}\lambda_2+q_{32}\lambda_1\right)+q_{32}\left(e_{32}\lambda_1+q_{32}\lambda_3\right)\right] \quad (A.22)$$

$$L_{29}=\frac{17h^3}{315}\left[e_{24}\left(e_{32}\lambda_2+q_{32}\lambda_1\right)+e_{15}\left(e_{32}\lambda_2+q_{32}\lambda_1\right)+q_{24}\left(e_{32}\lambda_1+q_{32}\lambda_3\right)+q_{15}\left(e_{32}\lambda_1+q_{32}\lambda_3\right)\right] \quad (A.23)$$

$$L_{30}=-\frac{8h}{15}C_{44}$$
$$L_{31}=\frac{17h^3}{315}\left[C_{12}+C_{66}+e_{31}\left(e_{32}\lambda_2+q_{32}\lambda_1\right)+q_{31}\left(e_{32}\lambda_1+q_{32}\lambda_3\right)\right] \quad (A.24)$$

$$L_{32}=\frac{17h^3}{315}\left[C_{22}+e_{32}\left(e_{32}\lambda_2+q_{32}\lambda_1\right)+q_{32}\left(e_{32}\lambda_1+q_{32}\lambda_3\right)\right] \quad (A.25)$$

$$L_{33}=\frac{17h^3}{315}\left[e_{24}\left(e_{32}\lambda_2+q_{32}\lambda_1\right)+q_{24}\left(e_{32}\lambda_1+q_{32}\lambda_3\right)\right] \quad (A.26)$$

$$L_{34}=\frac{17h^3}{315}\left[e_{15}\left(e_{32}\lambda_2+q_{32}\lambda_1\right)+q_{15}\left(e_{32}\lambda_1+q_{32}\lambda_3\right)\right] \quad (A.27)$$

## Appendix B

$$\gamma_1=-\frac{m^2\pi^2bh}{4a}L_1-\frac{n^2\pi^2ah}{4b}L_2+\frac{m^4\pi^4bh}{4a^3}L_8+\frac{n^4\pi^4ah}{4b^3}L_{14}+\frac{m^2n^2\pi^4h}{4ab}L_{10} \quad (B.1)$$

$$\gamma_2=-\frac{m\pi b}{4}L_4+\frac{m^3\pi^3b}{4a^2}L_6+\frac{mn^2\pi^3}{4b}L_{12} \quad (B.2)$$

$$\gamma_3=-\frac{n\pi a}{4}L_5+\frac{m^2n\pi^3}{4a}L_7+\frac{n^3\pi^3a}{4b^2}L_{13} \quad (B.3)$$

$$\gamma_4 = -\frac{m^3\pi^3 bh}{4a^2}L_{18} - \frac{mn^2\pi^3 h}{4b}L_{19} + \frac{m\pi bh}{4}L_{21} \qquad (B.4)$$

$$\gamma_5 = \frac{ab}{4}L_{21} - \frac{n^2\pi^2 a}{4b}L_{24} - \frac{m^2\pi^2 b}{4a}L_{25}$$
$$\gamma_6 = -\frac{mn\pi^2}{4}L_{26} \qquad (B.5)$$

$$\gamma_7 = -\frac{m^2 n\pi^3 h}{4a}L_{27} - \frac{n^3\pi^3 ah}{4b^2}L_{28} + \frac{n\pi ah}{4}L_{30}$$
$$\gamma_8 = -\frac{mn\pi^2}{4}L_{31} \qquad (B.6)$$

$$\gamma_9 = -\frac{m^2\pi^2 b}{4a}L_{24} + \frac{ab}{4}L_{30} - \frac{n^2\pi^2 a}{4b}L_{32} \qquad (B.7)$$

## References


[1] Brunelle EJ. Buckling of transversely isotropic Mindlin plates. *AIAA Journal* 1971; 9: 1018-22.

[2] Mizusawa T. Buckling of rectangular Mindlin plates with tapered thickness by the spline strip method. *Int J Solids Struct* 1993; 30: 1663-77.

[3] Dawe DJ, Wang S. Spline finite strip analysis of the buckling and vibration of rectangular composite laminated plates. *Int J Mech Sci* 1995; 37: 645-67.

[4] Wang W, Bert CW, Striz AG. Differential quadrature analysis of deflection, buckling, and free vibration of beams and rectangular plates. *Comput Struct* 1993; 48: 473-9.

[5] Teo TM, Liew KM. A differential quadrature procedure for three-dimensional buckling analysis of rectangular plates. *Int J Solids Struct* 1999; 36: 1149-68.

[6] Mohieddin Ghomshei MM, Mahmoudi A. Thermal buckling analysis of cross-ply laminated rectangular plates under nonuniform temperature distribution: A differential quadrature approach. *J Mech Sci Tech* 2010; 24: 2519-27.

[7] Wang X, Wang Y, Ge L. Accurate buckling analysis of thin rectangular plates under locally distributed compressive edge stresses. *Thin-Walled Struct* 2016; 100: 81-92.

[8] Wang X, Wang X, Shi X. Accurate buckling loads of thin rectangular plates under parabolic edge compressions by the differential quadrature method. *Int J Mech Sci* 2007; 49: 447-53.

[9] Cui S, Hao H, Cheong HK. Numerical analysis of dynamic buckling of rectangular plates subjected to intermediate-velocity impact. *Int J Impact Eng* 2001; 25(2): 147-67.

[10] Xiang Y, Wang CM. Exact buckling and vibration solutions for stepped rectangular plates. *J Sound Vib* 2002; 250(3): 503-17.

[11] Chen XL, Liew KM. Buckling of rectangular functionally graded material plates subjected to nonlinearly distributed in-plane edge loads. *Smart Mater Struct* 2004; 13(6): 1430-7.

[12] Wang D, Peng H. A Hermite reproducing kernel Galerkin meshfree approach for buckling analysis of thin plates. *Comput Mech* 2013; 51(6): 1013-29.

[13] Javaheri R, Eslami MR. Thermal buckling of functionally graded plates based on higher order theory. *J Thermal Stresses* 2002; 25(7): 603-25.

[14] Matsunaga H. Thermal buckling of functionally graded plates according to a 2D higher-order deformation theory. *Compos Struct* 2009; 90(1): 76-86.

[15] Selim S, Akbarov SD. FEM analysis of the three-dimensional buckling problem for a clamped thick rectangular plate made of a viscoelastic composite. *Mech Compos Mater* 2003; 39(6): 531-40.

[16] Ghorbanpour Arani A, Maghamikia Sh, Mohammadimehr M, Arefmanesh A. Buckling analysis of laminated composite rectangular plates reinforced by SWCNTs using analytical and finite element methods. *J Mech Sci Technol* 2011; 25(3): 809-20.

[17] Mohammadi M, Saidi AR, Jomehzadeh E. Levy solution for buckling analysis of functionally graded rectangular plates. *Appl Compos Mater* 2010; 17(2): 81-93.

[18] Kim SE, Thai HT, Lee J. Buckling analysis of plates using the two variable refined plate theory. *Thin-Walled Struct* 2009; 47(4): 455-62.

[19] Thai HT, Kim SE. Levy-type solution for buckling analysis of orthotropic plates based on two variable refined plate theory. *Compos Struct* 2011; 93(7): 1738-46.

[20] Bodaghi M, Saidi AR. Levy-type solution for buckling analysis of thick functionally graded rectangular plates based on the higher-order shear deformation plate theory. *Appl Math Model* 2010; 34(11): 3659-73.

[21] Thai HT, Vo TP. A new sinusoidal shear deformation theory for bending, buckling, and vibration of functionally graded plates. *Appl Math Model* 2013; 37(5): 3269-81.

[22] Kulkarni K, Singh BN, Maiti DK. Analytical solution for bending and buckling analysis of functionally graded plates using inverse trigonometric shear deformation theory. *Compos Struct* 2015; 134: 147-57.

[23] Bouazza M, Lairedj A, Benseddiq N, Khalki S. A refined hyperbolic shear deformation theory for thermal buckling analysis of cross-ply laminated plates. *Mech Res Commun* 2016; 73: 117-26.

[24] Grover N, Maiti DK, Singh BN. A new inverse hyperbolic shear deformation theory for static and buckling analysis of laminated composite and sandwich plates. *Compos Struct* 2013; 95: 667-75.

[25] Sayyad AS, Ghugal YM. Buckling and free vibration analysis of orthotropic plates by using exponential shear deformation theory. *Latin American J Solids Struct* 2014; 11(8): 1298-314.

[26] Fares ME, Zenkour AM. Buckling and free vibration of non-homogeneous composite cross-ply laminated plates with various plate theories. *Compos Struct* 1999; 44(4): 279-87.

[27] Zenkour AM. Buckling of fiber-reinforced viscoelastic composite plates using various plate theories. *J Eng Math* 2004; 50(1): 75-93.

[28] Ranjbaran A, Khoshravan MR, Kharazi M. Buckling analysis of sandwich plate using layerwise theory. *J Mech Sci Technol* 2014; 28(6): 2769-77.

[29] Cetkovic M. Thermal buckling of laminated composite plates using layerwise displacement model. *Compos Struct* 2016; 142: 238-53.

[30] Jabbari M, Farzaneh Joubaneh E, Khorshidvand AR, Eslami MR. Buckling analysis of porous circular plate with piezoelectric actuator layers under uniform radial compression. *Int J Mech Sci* 2013; 70: 50-6.

[31] Jandaghian AA, Rahmani O. On the buckling behavior of piezoelectric nanobeams: An exact solution. *J Mech Sci Technol* 2015; 29(8): 3175-82.

[32] Pan E. Exact solution for simply supported and multilayered magneto-electro-elastic plates. *J Appl Mech* 2001; 68(4): 608-18.

[33] Pan E, Heyliger PR. Free vibrations of simply supported and multilayered magneto-electro-elastic plates. *J Sound Vib* 2002; 252(3): 429-42.

[34] Xue CX, Pan E, Zhang SY, Chu HJ. Large deflection of a rectangular magnetoelectroelastic thin plate. *Mech Res Commun* 2011; 38(7): 518-23.

[35] Razavi S, Shooshtari A. Nonlinear free vibration of magneto-electro-elastic rectangular plates. *Compos Struct* 2015; 119: 377-84.

[36] Kattimani SC, Ray MC. Smart damping of geometrically nonlinear vibrations of magneto-electro-elastic plates. *Compos Struct* 2014; 114: 51-63.

[37] Xu XJ, Deng ZC, Zhang K, Meng JM. Surface effects on the bending, buckling and free vibration analysis of magneto-electro-elastic beams. *Acta Mech* 2016; 227(6): 1557-73.

[38] Li YS, Ma P, Wang W. Bending, buckling, and free vibration of magnetoelectroelastic nanobeam based on nonlocal theory. *J Intelligent Mater Sys Struct* 2016; 27(9): 1139-49.

[39] Li YS. Buckling analysis of magnetoelectroelastic plate resting on Pasternak elastic foundation. *Mech Res Commun* 2014; 56: 104-14.

[40] Kumaravel A, Ganesan N, Sethuraman R. Buckling and vibration analysis of layered and multiphase magneto-electro-elastic cylinders subjected to uniform thermal loading. *Multidiscipline Model Mater Struct* 2010; 6(4): 475-92.

[41] Lang Z, Xuewu L. Buckling and vibration analysis of functionally graded magneto-electro-thermo-elastic circular cylindrical shells. *Appl Math Model* 2013; 37(4): 2279-92.

[42] Ansari R, Gholami R, Rouhi H. Size-dependent nonlinear forced vibration analysis of magneto-electro-thermo-elastic Timoshenko nanobeams based upon the nonlocal elasticity theory. *Compos Struct* 2015; 126: 216-226.

[43] Ebrahimi F, Barati MR. Magneto-electro-elastic buckling analysis of nonlocal curved nanobeams. *Eur Phys J Plus* 2016; 131: 346 (13 pages).

[44] Jamalpoor A, Ahmadi-Savadkoohi A, Hosseini-Hashemi Sh. Free vibration and biaxial buckling analysis of magneto-electro-elastic microplate resting on visco-Pasternak substrate via modified strain gradient theory. *Smart Mater Struct* 2016; 25(10): 105035.

[45] Farajpour A, Hairi Yazdi MR, Rastgoo A, Loghmani M, Mohammadi M. Nonlocal nonlinear plate model for large amplitude vibration of magneto-electro-elastic nanoplates. *Compos Struct* 2016; 140: 323-336.

[46] Xu X, Deng Z, Zhang K, Meng J. Surface effects on the bending, buckling and free vibration analysis of magneto-electro-elastic beams. *Acta Mech* 2016; 227(6): 1557-1573.

[47] Liu J, Zhang P, Lin G, Wang W, Lu S. High order solutions for the magneto-electro-elastic plate with non-uniform materials. *Int J Mech Sci* 2016; 115-116: 532-551.

[48] Zhou Y, Zhu J. Vibration and bending analysis of multiferroic rectangular plates using third-order shear deformation theory. *Compos Struct* 2016; 153: 712-723.

[49] Wenjun W, Peng L, Feng J. Two-dimensional linear elasticity theory of magneto-electro-elastic plates considering surface and nonlocal effects for nanoscale device applications. *Smart Mater Struct* 2016; 25(9): 095026 (15 pages).

[50] Reddy JN. **Mechanics of laminated composite plates and shells: theory and analysis**. 2nd ed. CRC Press; 2004.

[51] Razavi S, Shooshtari A. Free vibration analysis of a magneto-electro-elastic doubly-curved shell resting on a Pasternak-type elastic foundation. *Smart Mater Struct* 2014; 23(10): 105003 (9 pages).

[52] Wu CP, Lu YC. A modified Pagano method for the 3D dynamic responses of functionally graded magneto-electro-elastic plates. *Compos Struct* 2009; 90(3): 363-72.